Experimental study of a thermochemical energy storage system operating at low temperature with ettringite-based materials

Noé Beaupere, Alexandre Malley-Ernewein, Tamar Nahhas, Stéphane Ginestet, Gabriel Samson, Martin Cyr

Solar Energy 282 (2024) 112927

Contents lists available at ScienceDirect

Solar Energy

journal homepage: www.elsevier.com/locate/solener

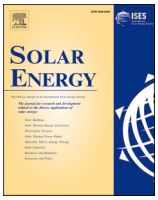

Experimental study of a thermochemical energy storage system operating at low temperature with ettringite-based materials

Noé Beaupere [2], Alexandre Malley-Ernewein [1], Tamar Nahhas, Stéphane Ginestet [*], Gabriel Samson, Martin Cyr

Université de Toulouse, UPS, INSA, LMDC (Laboratoire Matériaux et Durabilité des Constructions de Toulouse), 135, Avenue de Rangueil, 31 077 Toulouse cedex 4, France

ARTICLE INFO

Keywords:
Thermochemical energy storage
Ettringite cementitious material
Hydration-dehydration
Prototype

ABSTRACT

Cementitious material with a high ettringite content can be considered effective in a long-term (seasonal) thermochemical energy storage (TCES) system, resolving the issue of intermittency between production and availability of renewable energy. However, to evaluate the behavior of the storage material, an experimental study of energy storage in a thermochemical reactor containing the proposed material was required. A new and innovative large-scale energy storage prototype based on ettringite material has been developed and tested. This prototype regulates the temperature, humidity, flow rate, and pressure of the flow circulating through a 50 L CSA (calcium sulfoaluminate) sample monolith. This CSA cement formed an ettringitic phase ($3CaO\hat{A}\cdot Al_2O_3\hat{A}\cdot 3CaSO_4\hat{A}\cdot 32H_2O$) to store thermochemical energy at about 60 °C. After the storage cycle (high temperature, low relative humidity), the material was cooled down to room temperature and kept there until energy was needed. The stored energy was released on demand by the hydration of cement from a cold, humid nitrogen flow. About 50 MJ/m^3 was discharged from the 50 L monolith during the hydration cycle. The prototype showed the monolith's ability to store and release energy: the first discharge phase experimental test showed an energy release of about 10 % of the theoretical value (43 MJ/m^3) for a temperature increase of 6 K. Complementary investigations have to be performed to understand the impact of the monolith cracks on the energy performances.

1. Introduction

Renewable energy storage is now a topic that it is essential to address in connection with saving natural resources and reducing the environmental impact of buildings. Solar energy is a possible solution to reduce the dependence of the building sector on non-renewable energy. One of the main problems with the use of solar energy is its intermittent character. Thermal energy storage (TES) systems can bridge the phase shift between solar radiation and thermal energy demand. Thermal energy can be stored and used to produce electricity when renewable energy sources are unavailable or when the demand is high. Many energy storage materials have been used for this purpose [1].

This work presents a TES material based on cement foam. Cementitious materials are cheap, widely available construction materials, and present a facility of large volume production. They have thus been proposed for thermal heat storage based on the utilization of their relatively high specific heat capacity at a temperature of reaction adapted to the need for residential buildings. Their capability to store sensible heat with economic feasibility has been demonstrated for high temperatures [2,3,4] and the circulation of synthetic oil through cement has enabled large quantities of heat to be stored at up to 400 °C [5,6]. These materials can present thermochemical or sorption reactions with a high energy storage capacity.

Previous studies [7,8] led to the conception and the test of different prototypes using the reversible chemical reaction between ettringite, a cement compound, and water vapor to store heat. These two prototypes were based on small samples, with volumes of around 5 dm^3. The first one, based on a closed system, presents an efficiency of 42 % while the efficiency of the second one, based on an open system, was increased to 71 %. The novelty of this work is the development of an industrial-scale open system prototype using 50 dm^3 monolith cementitious material

* Corresponding author.
E-mail address: stephane.ginestet@insa-toulouse.fr (S. Ginestet).
[1] Present address: Universite Claude Bernard Lyon 1, CETHIL, UMR5008, CNRS, INSA Lyon, Villeurbanne F-69100, France.
[2] Present address: CY Cergy Paris Université, L2MGC, F-95000 Cergy, France

https://doi.org/10.1016/j.solener.2024.112927
Received 23 April 2024; Received in revised form 28 August 2024; Accepted 7 September 2024

Nomenclature

h	Enthalpy, J/kg
L_v	Heat of vaporization, J/kg
m	Mass, kg
p	Pressure, Pa
p_v	Vapor partial pressure, Pa
q	Transport gas flow, m^3/s
q_n	Normalized transport gas flow, m^3/s
t	Time, s
T	Temperature, K
w	Water vapor mixing ratio, kg_v/kg_{dtf}
φ	Relative humidity, %
ϕ	Porosity, %
ρ	Density, kg/m^3

Subscripts

dtg	Dry transport gas
mg	Moist gas
sat	Saturation
v	Vapor
0	Room temperature conditions
rel	Relative
wat	water
sol	solid

Abbreviations

CSA	Calcium sulfoaluminate
EMPA	Swiss Federal Laboratories for Materials Science and Technology
HTG	Heat transfer gas
LMDC	Laboratory for Materials and Durability of Constructions
PCM	Phase change materials
RH	Relative humidity
TES	Thermal energy storage
TCES	Thermochemical energy storage

instead of a powder.

The first part of the present paper is devoted to a historical review of the existing prototypes and materials able to store thermochemical energy in cementitious materials, leading to the choice of ettringite. The sample and the prototype designed for this study are described in Section 2. Equations for thermochemical energy storage are then detailed. Finally, the results are presented and discussed for energy storage in ettringitic cementitious material with the designed prototype.

2. Thermochemical reactors: description and principle

2.1. Different temperature ranges

The thermochemical heat storage (TCES) process materials have the advantage of high storage density compared to other thermal storage materials [9]. The TCES principle is to use a reversible chemical reaction between species to store heat: the reaction is endothermic in one sense and exothermic in the other, $A_{solid} + heat \leftrightarrow B_{solid} + C_{gas}$. In comparison with sensible and latent TES, this kind of storage does not present thermal energy losses while storing as the energy is not released until the two reactants come into contact.

The temperature of the reaction was one of the main parameters that influenced the performance of the selected material for thermochemical energy storage. Materials involved in TCES present a large variety of reaction temperatures [10]:

- 40–260 °C for dehydration/hydration of metal salt hydrates;
- 80–400 °C for dehydrogenation/hydrogenation of metal hydrides;
- 250–600 °C for dehydration/hydration of metal hydroxides;
- 100–950 °C for decarbonation/carbonation of metal carbonates;
- 600–1000 °C for deoxygenation/oxygenation of metal oxides.

Cementitious materials can store heat at different temperature levels:

- Portlandite ($Ca(OH)_2$) is a hydrate phase found in cementitious material capable of storing high amounts of thermal energy with a high storage temperature (500 °C) through sensible storage.
- Ettringite, a cement compound, presents high storage density at low temperatures (charging at less than 100 °C and discharging at around 60 °C) when reacting with water for TCES.

The temperature ranges showed by TCES with ettringite as a reactive material are easily reached using a conventional solar collector and correspond to the temperature of domestic hot water. Furthermore, in France, 50 % of the industrial heat waste is under 100 °C [11], which expands the domain of application with ettringite.

Thermochemical energy storage systems using low-temperature driven heat sources have received considerable attention due to their superior characteristics for seasonal heat storage (higher storage capacity, no heat loss) [12,13] compared to conventional sensible and latent heat technologies.

2.2. Summary of existing prototypes

This study mainly focused on using materials with high storage temperatures for thermochemical storage in building applications. Various thermochemical energy storage prototypes have been tested and presented in the literature. These prototypes had several implementation parameters (storage medium, storage volume, bulk density, porosity of bed texture, temperature and power of storage, and operating modes). The parameters and results of these different energy storage prototypes are presented in, which summarizes the different prototypes found in the literature and their properties. The materials presented here have a temperature of storage (thermochemical or sorption/desorption) suitable for building applications (below 200 °C).

Table 1 indicates that about 70 % of the prototypes had a bed energy density between 100 and 700 MJ/m^3. The highest values, up to 1650 MJ/m^3, were found for strontium-bromide [27] in a multiple beds open reactor configuration. Open systems generally exhibit higher energy density, in particular when the reactive material is displayed in beds, as accessibility to the reacting material is improved.

45 % of the prototypes are based on a combination of two or more reactive materials in order to enhance the system characteristics, mainly output temperature level and power. The discharging output power is an important parameter for future application but it is not available in all the studies and is barely used as a choice criterion.

Most of the prototypes contained powder of zeolites or salts, as their characteristics fit well with low-temperature applications. These materials had a high rate of energy release but low mechanical strength. Only one prototype used zeolite in a solid form and a few more used solid structures (reactive or not) impregnated with salts. When the materials were disposed in beds, agglomeration phenomena were often observed after several cycles, reducing the performances. Additionally, these materials had high prices, generally between 2000 and 5000 €/m^3 [14], which limits their use as domestic thermochemical energy material, while ettringite can be used as construction material.

More specifically, ettringite was found to have interesting properties that motivated its consideration for storage material in recent studies

Table 1
Summary of existing prototypes, partly adapted from [14]. NA: Not available.

Material used	Inlet temperature of charge, discharge, and temperature difference (outlet-inlet) during discharge	Internal volume	Bulk density	Material porosity	Discharge bed energy density	Storage capacity	Charging/discharging power	Type of system/reactive material form	Ref.
	/	dm^3	kg/m^3	/	MJ/m^3	MJ	kW	/	/
Data adapted from [14]									
LiCl/Water	T_{charge} = 40–85 °C $T_{discharge,i}$ = 25 °C ΔT_{o-i}=+5 K	16	1780	NA	910	126	15/8	Closed/solution	[15]
NaOH/Water	T_{charge} = 95–150 °C $T_{discharge,i}$ = 10 °C ΔT_{o-i}=+ 60 K	200	NA	NA	900	32.04	1/1	Closed / –	[16]
Silica gel/Water	T_{charge} = 88 °C $T_{discharge,i}$ = *NA* ΔT_{o-i} = *NA*	350	NA	NA	120	46.8	1 –1.5/0.5 –1	Closed/particles bed	[17]
Zeolite 13X/Water	T_{charge} = 110–180 °C $T_{discharge,i}$ = 65 °C ΔT_{o-i}=+6.2 K	NA	NA	NA	648	3.6	*NA*/0.8 –1.8	Closed/spherical particles bed	[14]
Zeolite 4A/Water	T_{charge} = 180 °C $T_{discharge,i}$ = 20 °C ΔT_{o-i}=+22 K	98	NA	NA	576	43.2	2 –2.5/1 –1.5	Open/honeycomb structures	[14]
Prototypes from other references									
Expanded natural graphite + $SrBr_2$/ Water	T_{charge} = 80 °C $T_{discharge,i}$ = *NA* ΔT_{o-i} = *NA*	1000	2386	NA	144	144	12/4	Closed/beds	[18]
Expanded natural graphite + LiCl/ Water	T_{charge} = 85 °C $T_{discharge,i}$ = 35 °C ΔT_{o-i}=+2.7 K	157	510	0.705	235	64.8	10/11.1	Closed/solution + bed	[19]
Expanded graphite + $MnCl_2/NH_3$	T_{charge} = 174 °C $T_{discharge,i}$ = 20 °C ΔT_{o-i}=+30 K	NA	NA	NA	NA	10.31	*NA*/*NA*	Closed/bed	[20]
Expanded graphite + $MgSO_4$/Water	T_{charge} = 85 °C $T_{discharge,i}$ = 23 °C ΔT_{o-i}=+5K	1.40	370	NA	225.63	0.32	*NA*/0.07	Closed/impregnated matrix (short term storage)	[21]
Silica gel/Water	T_{charge} = 110–118 °C $T_{discharge,i}$ = 28 °C ΔT_{o-i}=+18–32 K	NA	NA	NA	NA	NA	*NA*/*NA*	Closed/bed	[22]
$MgCl_2$ + Zeolite13X-4A/Water	T_{charge} = 95 °C $T_{discharge,i}$ = 23 °C ΔT_{o-i}=+3K	NA	NA	NA	NA	NA	*NA*/*NA*	Closed/plate fins	[23]
$MnCl_2$–$SrCl_2/NH_3$	T_{charge} = 177 °C $T_{discharge,i}$ = 45 °C ΔT_{o-i} = NA	NA	NA	NA	NA	7.66	*NA*/*NA*	Closed/packed bed	[24,25]
Zeolite 13X/Water	T_{charge} = 180 °C $T_{discharge,i}$ = 22–26 °C ΔT_{o-i}=+9.7 K	50	730	0.395	460.8	NA	*NA*/*NA*	Closed/copper fins	[26]
$SrBr_{2}$·/ Water	T_{charge} = NA $T_{discharge,i}$ = 21–25 °C ΔT_{o-i}=+20 K	90.25	NA	NA	10.66	NA	*NA*/0.270	Open/moving bed	[27]
$SrBr_2$/Water	T_{charge} = 80 °C $T_{discharge,i}$ = 12–30 °C ΔT_{o-i}= + 10.5 K	0.015	2390	0.64	1548–1650	NA	*NA*/*NA*	Open/beds	[28]

(*continued on next page*)

Table 1 (*continued*)

Material used	Inlet temperature of charge, discharge, and temperature difference (outlet-inlet) during discharge	Internal volume	Bulk density	Material porosity	Discharge bed energy density	Storage capacity	Charging/discharging power	Type of system/reactive material form	Ref.
	/	dm^3	kg/m^3	/	MJ/m^3	MJ	kW	/	/
$SrBr_2$·/ Water	T_{charge} = 80 °C $T_{discharge.i}$ = 25 °C ΔT_{o-i}=+ 9 K	271	2390	NA	1397	378	1.6/0.9	Open/beds	[29]
$MgCl_2$/Water	T_{charge} = 130 °C $T_{discharge.i}$ = 50 °C ΔT_{o-i}=+ 14 K	17	NA	0.50	500.4	NA	0.05/0.15	Open/packed bed	[30]
$SrBr_2$·/ Water	T_{charge} = 80 °C $T_{discharge.i}$ = 25 °C ΔT_{o-i}=+2.1 K	0.63	794	NA	136.74	2.01	*NA*/*NA*	Open/bed	[31]
K_2CO_3/Water	T_{charge} = 90 °C $T_{discharge.i}$ = 28.8 °C ΔT_{o-i}=+40.9 K	12.56	1432.39	NA	NA	NA	*NA*/*NA*	Open/vertical bed	[32]
Activated alumina and LiCl/Water	T_{charge} = 110 °C $T_{discharge.i}$ = 20 °C ΔT_{o-i}=+24.8 K	6	1116	0.29	687.6	3.6	*NA*/0.338	Open/vertical packed beds	[33]
$MnCl_2 - CaCl_2/NH_3$	T_{charge} = 92 °C $T_{discharge.i}$ = 40 °C ΔT_{o-i}=+15 K	8.14	538	NA	1006.6	8.19	*NA*/*NA*	Closed/packed bed	[34]
$MgSO_4$ + silica gel/ Water	T_{charge} = 110 °C $T_{discharge.i}$ = 50 °C ΔT_{o-i}=+57.4 K	1401	1070.7	NA	760	NA	*NA*/49.54	Closed/packed bed	[35]
Silica gel + $CaCl_2$/ Water	T_{charge} = 49.9–59.2 °C $T_{discharge.i}$ = 22.5–23.9 °C ΔT_{o-i}=+8.2 K (average)	163	13.49	NA	9.73	1.59	0.278/0.356(average)	Open/moving-vibrating bed with impregnated matrix	[36]
Silica gel/Water	T_{charge} = 120 °C $T_{discharge.i}$ = 20 °C ΔT_{o-i}=+ 21 K	4.7	720	NA	982.8	NA	*NA*/*NA*	Open/bed	[37]
Silica gel/Water	T_{charge} = 120–200 °C $T_{discharge.i}$ = 22 °C ΔT_{o-i}=+28.5 K	0.0628	803	NA	722.5	0.045	*NA*/0.0154	Open/particles column	[38]
Mesoporous silica + $CaCl_2$/Water	T_{charge} = 80–100 °C $T_{discharge.i}$ = 25 °C ΔT_{o-i}=+ 20.9 K	0.377	630	NA	950.4	0.36	*NA*/*NA*	Open/fluidized bed	[39]
Mesoporous silica + $MgBr_2$/Water	T_{charge} = 80–100 °C $T_{discharge.i}$ = 25 °C ΔT_{o-i}=+ 7.2 K	0.377	764	NA	352.8	0.13	*NA*/*NA*	Open/fluidized bed	[39]
Mesoporous silica + $MgSO_4$/Water	T_{charge} = 80–100 °C $T_{discharge.i}$ = 25 °C ΔT_{o-i}=+ 9.1 K	0.377	432	NA	158.4	0.05	*NA*/*NA*	Open/fluidized bed	[39]
Zeolite 13X − MgSO4/ Water	T_{charge} = 150 °C $T_{discharge.i}$ = 25 °C ΔT_{o-i}=+35 K	7100	2660 (powder: 500)	NA	598	2300.4	*NA*/0.006	Open/impregnated matrix	[40]
Zeolite 13X/Water	T_{charge} = 180 °C $T_{discharge.i}$ = 55 °C ΔT_{o-i}=+75 K	114.75	1481.48	NA	490	194.4	*NA*/4.4	Open/four bed segments	[41,42]
Zeolite 13X+$SrCl_2$-cement/Water (long-term)	T_{charge} = 130 °C $T_{discharge.i}$ = NA ΔT_{o-i} = 23 °C	0.27	NA	0.41 (zeolite) 0.43 (cement)	496.44	0.13	*NA*/0.009	Open/cascade particles bed	[43]

(*continued on next page*)

Table 1 (*continued*)

Material used	Inlet temperature of charge, discharge, and temperature difference (outlet-inlet) during discharge	Internal volume	Bulk density	Material porosity	Discharge bed energy density	Storage capacity	Charging/discharging power	Type of system/reactive material form	Ref.
/	/	dm^3	kg/m^3	/	MJ/m^3	MJ	kW	/	/
Zeolite 13X+$SrCl_2$-cement/Water (short-term)	T_{charge} = 130 °C $T_{discharge,i}$ = NA ΔT_{o-i} = 23 °C	0.27	NA	0.41 (zeolite) 0.43 (cement)	352.44	0.09	*NA*/0.009	Open/cascade particles bed	[43]
Prototypes based on ettringitic materials									
Ettringite/Water (prototype 1)	T_{charge} = 60 °C $T_{discharge,i}$ = 20 °C ΔT_{o-i} =+22 K	4.9	NA	0.76	219.6	1.08	0.02/0.002	Closed/solid cylinder	[8]
Ettringite/Water	T_{charge} = 60–83 °C $T_{discharge,i}$ = 10 °C ΔT_{o-i} =+ 22 K	6000	1220	0.25	216	1296	*NA*/*NA*	Closed/solid layers	[44,45]
Ettringite/Water (prototype 2)	T_{charge} = 60 °C $T_{discharge,i}$ = 19 °C ΔT_{o-i} =+ 16 K	6.5	409	0.76	421.2	2.74	0.05/0.009	Open/solid cylinder	[8]
Ettringite/Water	T_{charge} = 75–95 °C $T_{discharge,i}$ = 15–20 °C ΔT_{o-i} =+ 39.4 K	0.05	NA	NA	374.4	0.019	0.05/0.045	Open/bed	[46]

[7,47,48]. These properties were a compressive strength of 2 MPa after a foaming process, a relative density of 0.9, and a low temperature required for thermochemical storage (60 °C). In addition, bed storage energy density was equivalent to that of other materials, between about 200 and 400 MJ/m^3. However, the carbonation of such materials must be managed [47].

2.3. The choice of ettringite

Ettringite ($3CaO\hat{A}\cdot Al_2O_3\hat{A}\cdot 3CaSO_4\hat{A}\cdot 32H_2O$) is a hydrate found in several cementitious materials. It constitutes a small percentage of Portland cement, while calcium sulfoaluminate (CSA) cement usually contains higher amounts (40–80 %) [47]. Ettringite is produced from ye'elimite ($CaO\hat{A}\cdot 3Al_2O_3\hat{A}\cdot SO_3$) and anhydrite ($CaSO_4$) hydration based on Eq. (1)

$$4CaO\hat{A}\cdot 3Al_2O_3\hat{A}\cdot SO_3 + 2CaSO_4 + 38H_2O \rightarrow 3CaO\hat{A}\cdot Al_2O_3\hat{A}\cdot 3CaSO_4\hat{A}\cdot 32H_2O + 4Al(OH)_3 \quad (1)$$

Struble et al. [49] were the first to consider ettringite as a potential candidate for thermochemical energy storage in 1986 but interest in the subject has risen in the last decade [50]. Its main advantages are a lower cost than other thermochemical storage materials, low toxicity, and high heat storage density (about 1400 MJ/m^3) at low temperatures (around 60 °C) [14,48].

This material also presents a high specific heat (1260 J/(kg.K)) and a molar mass of 1309.3 g/mol [49]. The endothermic reaction of thermochemical storage is the dehydration (water desorption) of ettringite to give meta-ettringite ($3CaO\hat{A}\cdot Al_2O_3\hat{A}\cdot 3CaSO_4\hat{A}\cdot 12H_2O$), related to the loss of about 20 water molecules. These molecules are bound by weak intramolecular (Van der Waals forces) and hydrogen bonding [47] that can be easily broken by elevation of the temperature, following Eq. (2).

$$3CaO\hat{A}\cdot Al_2O_3\hat{A}\cdot 3CaSO_4\hat{A}\cdot 32H_2O + \text{heat} \leftrightarrow 3CaO\hat{A}\cdot Al_2O_3\hat{A}\cdot 3CaSO_4\hat{A}\cdot 12H_2O + 20\,H_2O \quad (2)$$

During charging, the heat is consumed by the desorption reaction (conversion of ettringite to meta-ettringite). Energy remains stored as long as the material is kept away from water (and CO_2), either for short-term (daily, weekly) or long-term (seasonal) storage. When energy is needed, water is brought into contact with meta-ettringite, triggering a chemical reaction (adsorption or hydration) and a significant release of heat on demand.

Different prototypes, ranging from small to large scale, made with ettringite material as seasonal storage material, have been studied. First, a study was conducted at EMPA [50], where ettringite was used as a storage material for a high volume (6 m^3). Kaufmann et al. [45] tested several prototypes using ettringite as thermal energy storage material. Their study mainly focused on a system that contained 24 separate blocks of 400 kg each, for a total volume of 6 m^3 of ettringite. The modules were connected to the house heat distribution system by copper pipes. In parallel, 20 m^2 of solar panels were installed, increasing the temperature of a 9 m^3 water tank to a maximum of 85 °C (sensible heat storage). In addition, they were able to heat the ettringite to 80 °C during summer, leading to its dehydration (charging phase). This first sensible heat storage prototype ensured good thermal comfort until winter, when the heat release from ettringite was triggered by hydration (discharging phase). The authors showed the ability of ettringite to store energy without cracking (which could have degraded the system's effectiveness).

Two previous experimental prototypes have also been built at LMDC [8] to investigate the heat storage performance of a thermochemical reactor with ettringite material. The first consisted of a cylindrical axial metal tube (closed configuration, Fig. 1 (a)) surrounded by ettringite

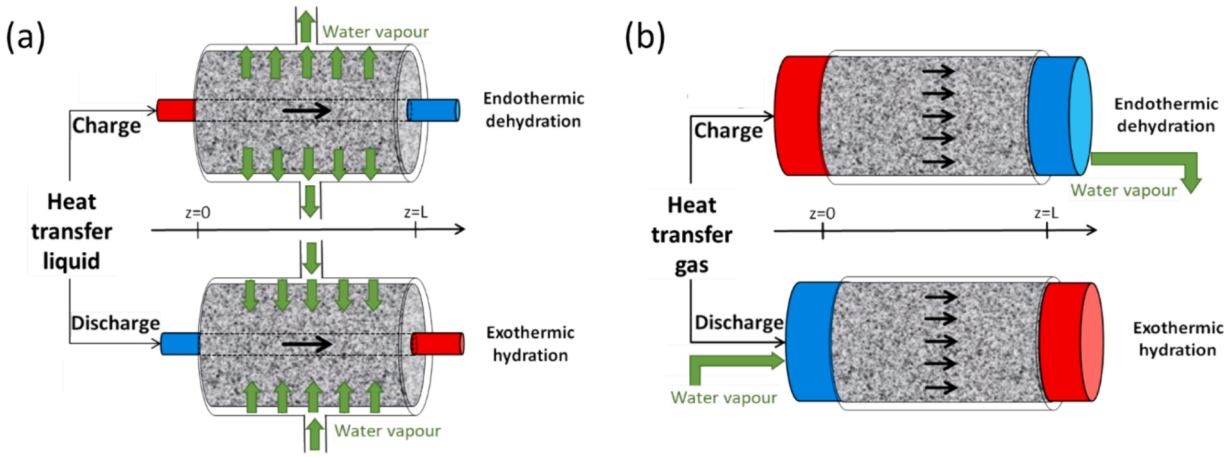

Fig. 1. Prototype designs, (a) closed configuration and (b) open configuration [8].

material as a path for heat transfer fluid. A second circuit was devoted to incoming and outgoing water to hydrate meta-ettringite and dehydrate ettringite. Thermocouples and relative humidity sensors were used to measure the hydrothermal evolution within the ettringite material during charging and discharging cycles. They showed a heat storage yield of 44 % or a storage capacity of 221 MJ/m^3, similar to the data from [45,50].

The second prototype was developed to improve the heat storage performance of the thermochemical reactor, in accordance with previous observations (see Table 1). Without the metal tube, this prototype used a single gaseous phase (open configuration, Fig. 1 (b)) in direct contact with the ettringite material (porous network). This gas was the heat transfer fluid in the charging phase and the humidifying gas in the discharging phase. The water vapor in the open system allowed better diffusion in the material and an increase of efficiency from 44 % to 71 %, with a storage density of 421.2 MJ/m^3 during discharge. Therefore, it was this prototype that was upscaled in the present work.

2.4. The particular issue of carbonation

The main problem with using ettringite as a thermochemical storage material is its carbonation [47]. In the presence of carbon dioxide, the ettringite decomposes over time into calcite, gypsum, and alumina gel (Eq. (3)).

$$3CaO \bullet Al_2O_3 \bullet 3CaSO_4 \bullet 32H_2O + 3\,CO_2 \rightarrow 3\,CaSO_4 \bullet 2H_2O + 3\,CaCO_3 + 2\,Al(OH)_3 + 23\,H_2O \quad (3)$$

Recently, Chen et al. observed that the degradation of ettringite occurred in a few hours at 70–90 % RH, while it was not significant below 50 % RH [51]. In this perspective, many research studies have been conducted in order to investigate the stability of ettringite under the operational conditions of energy storage. On the one hand, the results presented by Xiantuo et al. [52] showed that, at low relative humidity and constant partial pressure of H_2O and CO_2, the carbonation rate decreased with increasing temperature. On the other hand, at constant CO_2 pressure and 100 % RH, the carbonation rate increased with rising temperature. In the same context, Nishikawa et al. [53] conducted experiments on the stability of ettringite in contact with CO_2. They found that, with a high-water vapor concentration, ettringite decomposed in the air over time to form calcium carbonate, gypsum, and alumina gel, while the carbonation without water led to only slight compositional changes. To sum up, it is necessary to protect ettringite from CO_2 to ensure its stability if it is used as a thermochemical storage material. This protection from CO_2 can be achieved by using a membrane that filters carbon dioxide from the air at the prototype inlet, separating nitrogen from oxygen and carbon dioxide by activated carbon, or by using a closed-loop heat storage system under moist nitrogen gas instead of moist air [47]. The impact of exposing pure ettringite to carbon dioxide (CO_2 concentration at 400 ppm) was experimented by Grounds et al. [54]. Several temperatures (25 °C, 50 °C, 75 °C, and 95 °C) were tested with 100 % of relative humidity. At 25 °C, complete decomposition of ettringite was observed after two months of storage, while this duration tended to be significantly reduced with an increase in temperature.

2.5. Effect of temperature on the durability of ettringite

Zhou and Glasser [55] showed that the conversion of pure ettringite into meta-ettringite increased exponentially with water vapor pressure and temperature. It was demonstrated that this conversion was more important at 57 °C with 21.5 molecules of water released than at 50 °C

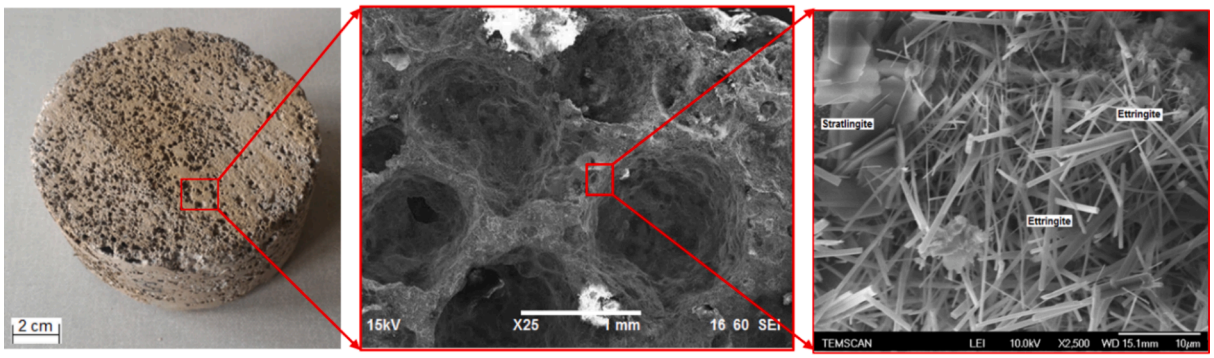

Fig. 2. Microstructure of the foamed material, from macro to micro scale with an SEM microscope (JEOL/EDS Bruker) [8].

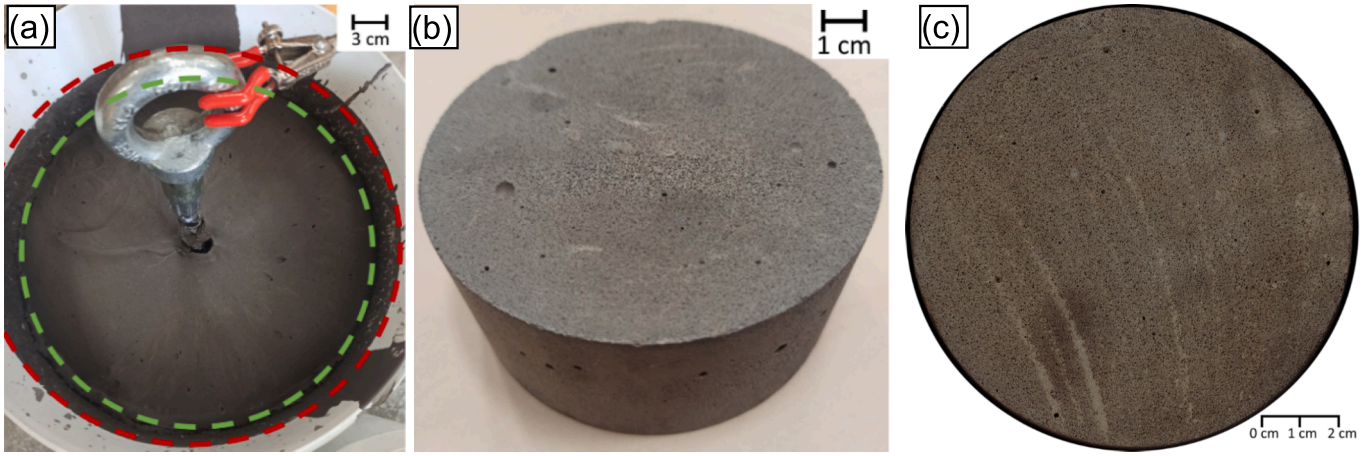

Fig. 3. (a) Collapse during casting of a highly porous concrete (density of 600 kg/m^3). Red and green circles correspond to the foam before and after the collapse, respectively; small scale sample of the material prepared for this study (porosity of 53 %, density of 0.869) as (b) photo and (c) scan of the surface.

with 19.3 molecules involved. Drying at only 40 °C induced the loss of 2 water molecules in the ettringite, whose quantity moved from 32 molecules to 30. The authors also explored the instability of ettringite at temperatures above 100 °C. In 2016, Ndiaye [56] proved that the stability of ettringite material depended strongly on the environmental conditions of conservation (presence of CO_2, temperature, and relative humidity). After several cycles, the carbonation, thermal stability, and reversibility of the ettringite/meta-ettringite transformation were measured, revealing that the ettringite lost its crystallinity at around 60 °C under low water vapor pressure (75 Pa to 200 Pa). After three days at 60 °C, the ettringite had lost 18 molecules of water; it was wholly converted to meta-ettringite, which contains 12 molecules of water.

3. Experimental Investigation

In order to enhance comprehension of the behavior of TCES systems, a new large-scale prototype has been designed and built. Studies using this prototype had two main objectives. First, they aimed to determine the influence of a scale-up of the material, a monolithic ettringite-based system, and to understand:

- The durability of the material (carbonation of ettringite, material cracking, mechanical strength) with various operational conditions;
- The influence of the physical properties of the environment (temperature, humidity, pressure, flow) and the material (density, permeability) on the behavior during charging/discharging steps;
- The effect of these material properties and durability on the global yield of the system.

Secondly, the energy efficiency of the system was studied in detail to understand the real behavior energy balance of the device. Previous prototypes [8] served as proof of concept, while the new one was designed to explore a large-scale system and understand its global functioning.

3.1. Interest in an aerated material from foaming

Although Portland cement is generally used for construction, it contains small quantities of ettringite. Using sulfoaluminate binders (CSA cement and anhydrite) was thus preferred, as their ettringite content could reach 65–70 % [7]. In order to accelerate the absorption and release of water, which directly impacts heat storage and release, an aerated cementitious material was produced.

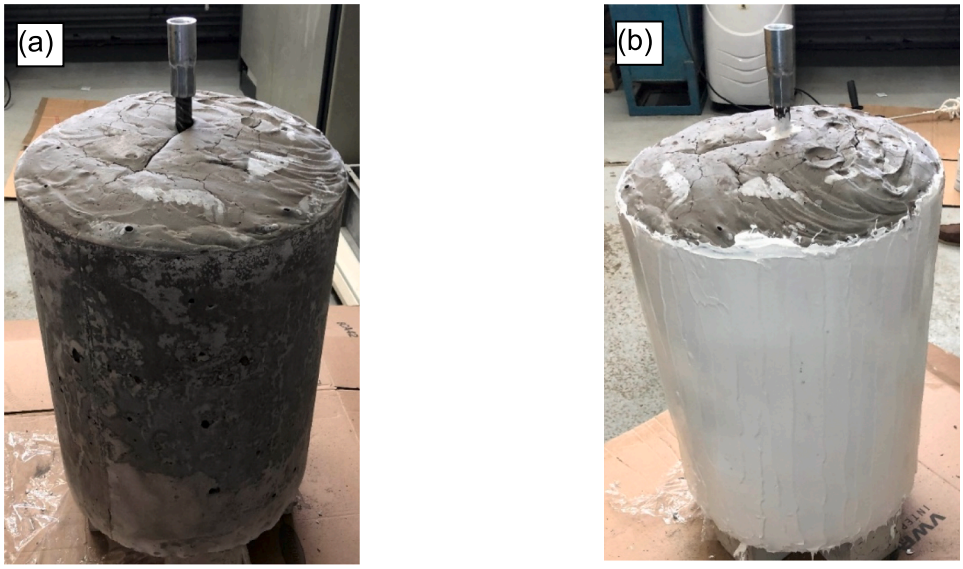

Fig. 4. Cylindrical monolith – (a) after removal of the formwork and (b) after resining.

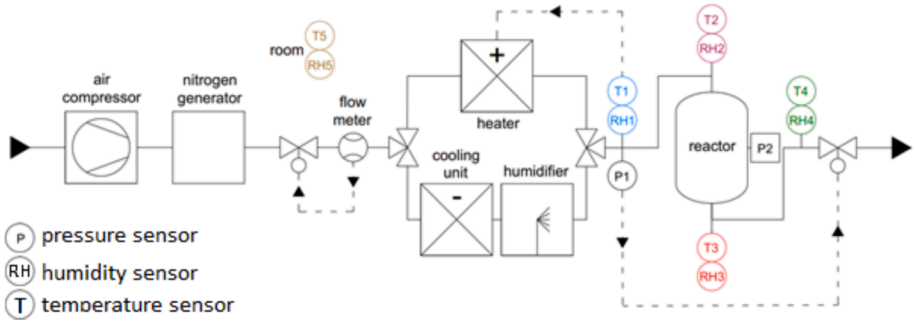

Fig. 5. Schematic description of the different functions of the prototype. These functions are described in the appendix (Table A. 1 and Figure A. 1). The dashed path with arrows corresponds to the retroaction of the measurement of flow, pressure, or heating, of nitrogen. The colors of the sensors correspond to their curves in the following figures.

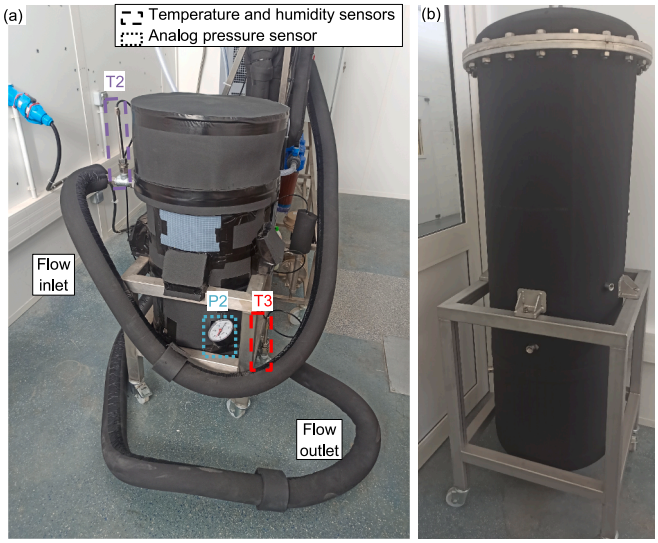

Fig. 6. (a) 50 dm^3 insulated reactor connected to the nitrogen network with temperature/humidity and pressure sensors and (b) 250 dm^3 reactor with almost no insulation.

It was shown that an aerated material (porosity up to 76 %) may lead to an increase in heat storage yield from 44 to 71 % based on previous work [7] with a storage density of 117 kWh/m^3. This aerated material was obtained from foaming by releasing hydrogen gas during the reaction of the binder. Thus, the specific area was increased, favoring the thermochemical reaction while maintaining acceptable mechanical properties. A compressive strength of 2 MPa was found for the material used for the two previous prototypes at lab scales, whose microstructure is given in Fig. 2 at different scales.

3.2. Scale-up of the foam storage material

In the present study, the chemical foaming process was obtained by the addition of hydrogen peroxide (35 %, J.T. Baker®, 1 L). Special attention was given to the number, size and connection of cavities from the hydrogen reaction had to be significant to ensure the circulation of the vapor flow during the energy storage process. Tests were first performed to reproduce the porosity of 76 % (Fig. 2) in a large-scale prototype (50 L instead of 1 L). However, the fresh foam collapsed before the material set (Fig. 3 (a)). This collapse may have been due to coalescence between bubbles. Therefore, cementitious material with reduced porosity was produced for this scale-up as a compromise between fresh foam stability until setting and good gas permeability in the hardened foam.

The cement paste was obtained by mixing sulfo aluminate cement (Vicat Alpenat R^2), water (E/C ratio of 0.43) and hydrogen peroxide. It was poured into the monolith mould (0.05 dm^3) and two 11x22 (diameter × height) cardboard moulds for characterization. The surface was covered and the material was left at room temperature of about 20 °C for 28 days. Fig. 3 (b) and (c) presents an 11x22 sample that was cut at mid-height to show the distribution of porosities.

The apparent density was determined by Eq. (4)

$$\rho = m/V \tag{4}$$

With ρ the apparent density (kg/m^3), m the mass (kg) and V the volume (m^3), with a density of about 869 kg/m^3. In parallel, the porosity was determined following the NF P 18-459 standard [57]. The samples presented in Fig. 3 (b) were first placed in a vacuum desiccator for 3 h, then water was added to fill the pores. As the samples were lighter, they were ballasted to be maintained in immersion. The samples were left immersed for 14 days, then placed on a hydrostatic balance, and a mass M_{water} was measured. The samples were taken out, the superficial water was wiped and a second value was found as M_{air}. To evaporate the residual water, the samples were left in a climate chamber for 7 days and a third mass, namely M_{dry}, was obtained. The open porosity ϕ (%) of the sample can be calculated from these three masses, following Eq. (5).

$$\phi = 100 \times (M_{air} - M_{dry})/(M_{air} - M_{water}) \tag{5}$$

The open porosity value was found to be about 53 %. Compressive strength was measured by a 100 kN universal press (IGM, 100 kN), and found to be about 3.5 MPa.

To find the heat capacity, 12 mg of ettringite was heated from 0 to 270 °C at 10 K/min with a differential scanning calorimetry device (NETZSCH, STA 449F3), and a heat capacity of 1260 $J.kg^{-1}.K^{-1}$ was found at 20 °C. This value was 30 % lower than the literature data [58], consistent with the presence of porosities in the material and the precision of the equipment.

The cylindrical monolith, from the same batch, presents a diameter after hydration of about 33 cm and a height of approximately 50 cm. Thus, its volume was approximately 0.043 m^3 (Fig. 4 (a)). These dimensions depended on two constraints: the monolith diameter dimension was fixed by the reactor's internal size (see paragraph 3.3), and its height was set by the chemical foaming process (see the previous paragraph). The mass of the sample was 36.88 kg (Mettler Toledo, Model BBA236-4B150N, precision of ±20 g). The monolith sidewall was coated with epoxy resin to force the flow to cross the reactive material from top to bottom (Fig. 4 (b)).

3.3. Design of the system

The energy storage capacity of the foamed ettringite (Fig. 4 (a)) was evaluated by the new prototype developed for this study. The schematic description of the prototype is presented in Fig. 6. It was designed to

Table 2
Description of the sensors used. Precision of humidity sensors are only valid between 10 and 90 %RH. The abbreviations of sensors correspond to their positions in Fig. 6.

Abbreviation	Designation	Model	Fabricant	Precision (datasheet)	deviation σ* (measured)
–	Flowmeter	MCF0250AGND0100D0	Azbil	±3 %	–
P1	Manometer	Premasgard SHD-SD-I 10	S+S Regeltechnik	±0,3 %	–
P2	Manometer	232.50	WIKA		–
T1/RH1	Temperature/ humidity sensor	SZKA.ED.F159.313.1KH	Galltec + mela	±0.15 K ±1.5 %RH	±0.03 K ±0.4 %RH
T2/RH2	Temperature/ humidity sensor	SZKA.ED.F159.313.1KH	Galltec + mela	±0.15 K ±1.5 %RH	±0.06 K ±0.5 %RH
T3/RH3	Temperature/ humidity sensor	SZKA.ED.F159.313.1KH	Galltec + mela	±0.15 K ±1.5 %RH	±0.04 K ±0.5 %RH
T4/RH4	Temperature/ humidity sensor	SZKA.ED.F159.313.1KH	Galltec + mela	±0.15 K ±1.5 %RH	±0.06 K ±0.4 %RH
T5/RH5	Temperature/ humidity sensor	KH-50	KIMO	±0.4 K ±2.5 %RH	–

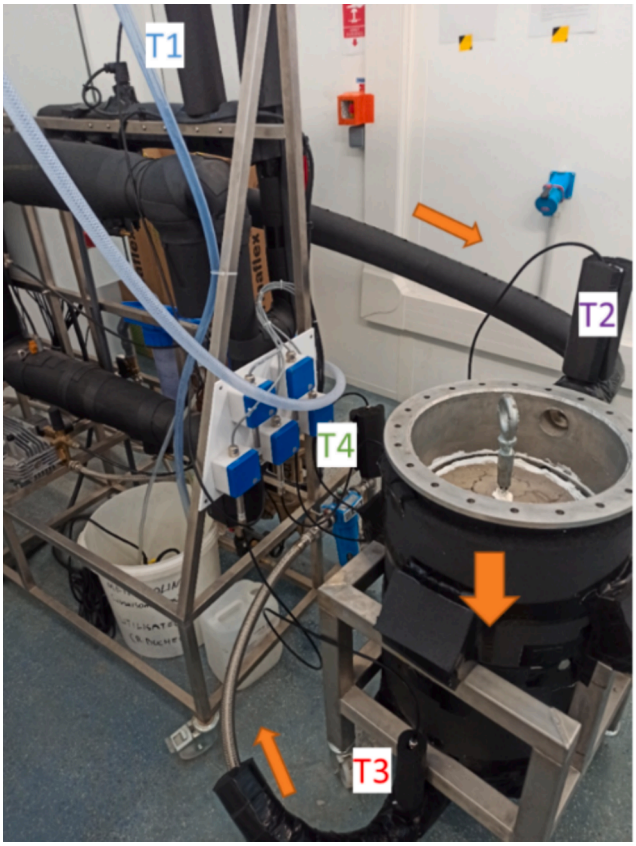

Fig. 7. Photo with the distribution of the Pt100/humidity sensors (T1, T2, T3, and T4). The arrows represent the direction of the gas flow. The font colors correspond to the color of the curves in the following figures.

explore the material's influence and the system's efficiency by controlling the different experimental parameters. To produce the heat transfer fluid (HTF), ambient air is compressed by an air compressor and, if necessary, its carbon dioxide is extracted with a nitrogen generator. HTF gas flow rate and pressure are controlled thanks to three-way hydraulic valves positioned after the nitrogen generator and at the prototype outlet. The HTF can be directed toward a heater to obtain a hot dry gas, leading to the dehydration of ettringite (energy storage) or towards a cooling unit and hydration system to obtain cold humid gas in order to release energy from the reactive material. This setup was used to test the capacity of ettringite to store and release thermal energy (detailed description in Appendix).

Measurements of the temperature, humidity, pressure, and gas flow were recovered using a programmable logic controller. This controller also drove the heating temperature and pressure by PID regulation. PID regulation of the gas flow was possible but not considered in this study as it could interfere with regulating pressure. Two hydraulic valves were available in the prototype to control either gas pressure or gas flow.

3.3.1. Gas generation adapted to the material properties

Two gases were selected for this study: air and nitrogen flow. Air was chosen as it was suitable for building applications, such as storage based on mechanical ventilation. However, it could lead to the carbonation of ettringite material and decreased storage capacity. A nitrogen environment could be preferred when a non-aggressive atmosphere is considered, such as for heat recovery in industrial applications. As presented before, the prototype components allow the production of compressed air (10 bars, 100 m^3/h) and compressed nitrogen (8 bars, 12 m^3/h, 95 % purity). The dryer is used to avoid water contamination in the nitrogen generator. It can also limit the moisture in heat transport gas and thus the unwanted release of energy with the hydration of ettringite.

3.3.2. Management of the heat transport gas characteristics

In order to cover the largest range of temperature and humidity, several devices were installed in the system: an electric heater (20 kW), a refrigeration unit (0.65 kW), and a humidifier (0.278 mg/s of water purified by several filters and injected by nozzles). As the nitrogen flow was mixed with water from nozzles, the humidity of the gas increased adiabatically, resulting in a decrease in the temperature.

Two paths were available. The first was composed of a heater, where a dry (below 20 % RH) and hot (up to 80 °C) gas flow was produced to dehydrate the material (Fig. 6). In the second branch, humid (above 70 % RH) and cold (below 10 °C) air/nitrogen flow could be obtained to release the energy stored in the meta-ettringite.

All the powers of the different elements were measured by wattmeters to estimate the electric energy consumption of the prototype. This measurement was made to ensure that this consumption was below the storage capacity, thus validating the use of the technology for energy storage.

3.3.3. Reactor design

Previous prototypes [8] were designed to serve as proof of concept, with a relatively small size (4.9 and 6.5 dm^3). The new prototype was equipped with two different cells of 50 dm^3 and 250 dm^3, as presented in Fig. 6. This allowed the energy storage and its reversibility to be validated at a larger scale.

The reactors are equipped with a cover, easily openable for installation of the sample. The thermal insulation for the 50 dm3 reactor (left) was reinforced by 32 mm Armaflex to limit heat loss, whereas the 250 dm3 (right) only had initial thermal insulation of 13 mm. For experiments, the gas pipes were shortened to limit heat loss, and the reactor was turned by 180° (inlet on the right and outlet on the left) in the

following pictures.

3.3.4. Monitoring of the gas properties

Table 2 presents all the sensors implemented on the prototype and used to monitor the properties of the HTF. This table inventories the sensors' types, model and brand, measurement characteristics, and abbreviations used in this study.

Deviations of temperature and humidity sensors, given in Table 2, were found by immersing the probes in 4 controlled ambiences, respectively thermostatic bath and saline solutions, during 24 h (3 s sampling). Calibration equipment was not available for other sensors, whose data were not deeply analyzed. As described before, the controller drives the heating temperature and pressure through a PID regulation, which adds an uncertainty of ±0.5 K and ±0.03 bar around the setpoint, respectively.

- Temperature and humidity ranges

In this reactor, several temperature/humidity probes could be inserted. The temperature and humidity monitoring were carried out with four Pt100 probes (Galltec-Mela, AWK with SZKA-series). Six positions were available, distributed vertically and radially over the reactor, for their installation. However, the study of a monolith made the insertion of probes difficult. Instead of being inserted in the reactor, two sensors were installed immediately before and after the reactor (T2 and T3), and two were on the pipes farther than 1 m from the reactor (T1 and T4). As the full insertion of the sensors in contact with the fluid would be more relevant, they were expected for further studies but not considered here due to technological issues. They are labelled in Fig. 7, and the direction of gas flow through the prototype is indicated by orange arrows.

The precision of the different probes was verified by immersing the Pt100 sensors in a thermostatic bath at 20, 45, 60, and 75 °C for 5 min with an acquisition every 3 s. For humidity, the probes were positioned close to various saturated salt solutions (NaOH, LiCl, $MgCl_2$, and NaCl) near the sensors. Uncertainties of up to 0.25 K (temperature) and 2 % RH (humidity) were found for the different probes. The sensors were insulated to limit the influence of room temperature and direct solar irradiance.

- Pressure measurement

The maximum allowable pressure in the prototype was 10 bar, which was the acceptable limit for airflow. Nitrogen flow was limited to 8 bars, as 20 % of the air (oxygen) was taken out by the nitrogen generator. This pressure was monitored by a numerical manometer (S+S Regeltechnik, Premasgard SHD-SD) positioned close to temperature/

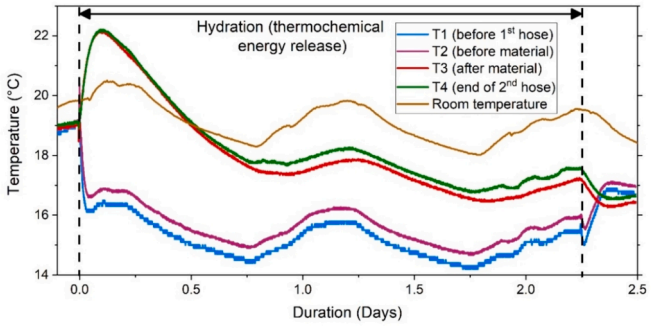

Fig. 9. Detailed view of the hydration step (blue rectangle from Fig. 8 (a)).

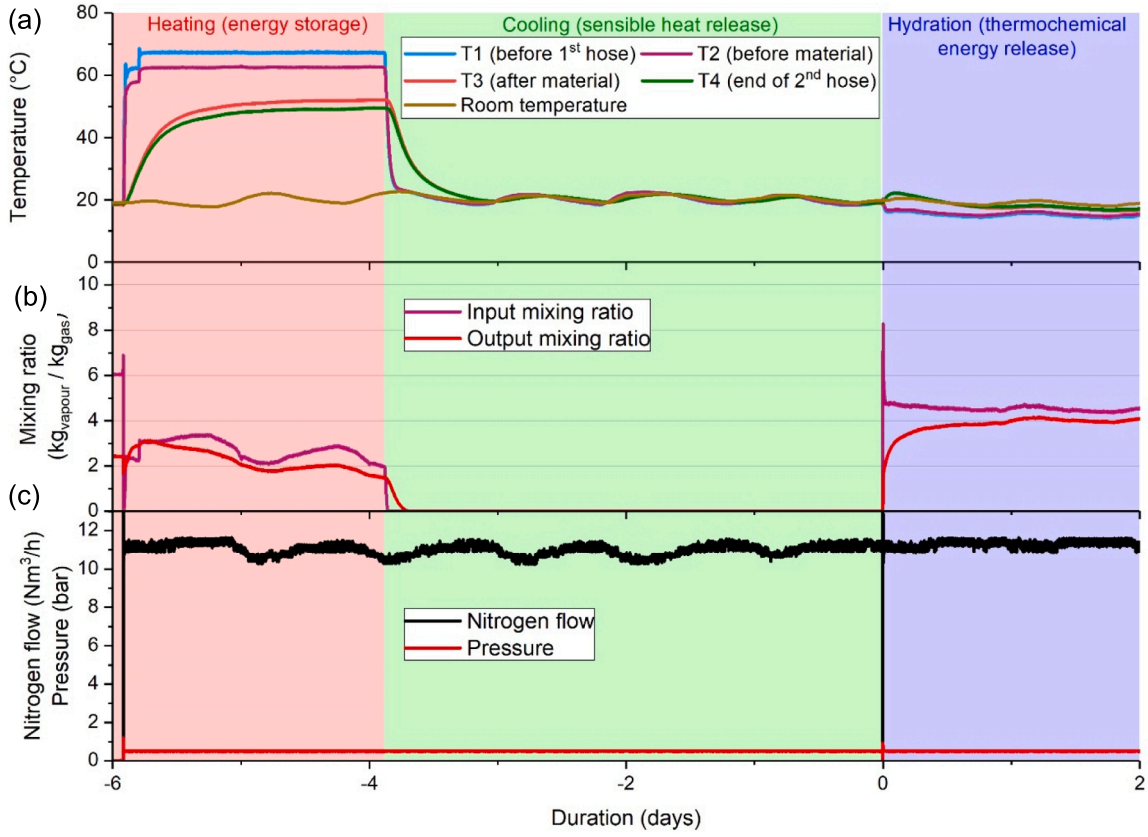

Fig. 8. Evolution through the different steps (heating, cooling, and hydration of the cementitious material) of (a) temperatures, (b) Mixing ratios and (c) nitrogen flow and pressure.

humidity sensor T1 (see Fig. 5). The pressure measurement was consistent with that from a second, analog, manometer P2 (WIKA, Type 111.10 manometer) in contact with the reactor (see Fig. 6 (a)). An analogic manometer (WIKA EN837-1) was placed at the reactor output in order to control the order of magnitude of the pressure drop through the material.

- Gas flow management

The gas flow was monitored by a thermal mass flowmeter (Azbil, MCF Series) positioned immediately after the gas production unit (see Fig. 5). The system was driven by a gas flow that crossed the material sample. The system was designed to ensure a large gas rate, from 0 to 100 m^3/h (with air) and 12 m^3/h (with nitrogen). This normalized flow rate value, q_n, did not depend on pressure, as it was based on the relative ambient pressure of 0 Pa, according to the ISO 1217 standard [59], given by Eq (6):

$$q_n = q \times (p_0 + p_{rel}) \quad (6)$$

where p_0 and p_{rel} are the ambient and relative pressure, and q is the gas flow at the relative pressure p_{rel}. In this study, an increase in pressure p_{rel} would lead to the decrease of gas flow q, the normalized flow (q_n) being constant. The prototype design was done in parallel with the reactive material design, thus monoliths height, permeability and so pressure drop were estimated. The prototype components were selected to be able to cover a large range of flow rates and pressure drops.

4. Results and discussion

4.1. Energy storage and release

Before exploiting the data from the prototype to evaluate its storage capacity, the characteristics of the heat transfer gas (HTG) had to be defined. They are linked to the experimental values measured by the sensors (relative humidity, temperature, and pressure). As presented above, due to the material specification, the HTF was moist nitrogen for carbonation avoidance, i.e. gaseous dry nitrogen plus water vapor. The equations given in the appendix (see Section A.2) are written for all the possible cases, which means using moist nitrogen or air. The results presented are issued from the last of three tests (namely "test 3"), the supplementary data from the different tests may be found in the appendix (Section A.3).

In the first part, the cycle is developed to be representative of the real behavior of a storage system based on cementitious material:

- The first step consists of energy storage by dehydration and endothermic transformation of the ettringite to meta-ettringite thanks to hot and dry HTF.
- The second step was intended to cool the ettringite under HTF until ambient temperature for the demonstration of long-term storage.
- The third step (discharge of heat) was associated with the hydration of meta-ettringite by a nitrogen-water vapour gas flow.

In the second part, the energy released was determined, using measurements of temperature, pressure, gas flow and humidity ratio.

4.1.1. Temperature and humidity evolution for a complete cycle

A reproduction of the experimental conditions of Ndiaye et al. [7] was first intended, as they found high values for heat recovery (up to 421 MJ/m^3). The process was divided into three steps (Fig. 8), with the time set at 0 at the beginning of the last step (release of heat). The relative pressure was set at 0.5 bars.

For the first step, the heating system was used to heat the nitrogen flow (10 m^3/h) to a temperature of 70 °C while maintaining low humidity, below 5 % RH. This setting was a good compromise for complete dehydration of the ettringite, but without permanently damaging the material (as a high temperature above 65 °C was assumed to destabilize the ettringite) [55]. In Fig. 8 (a), the temperature has been found, empirically, to give a temperature of 68 °C before the first hose (blue curve, T1), 62 °C before (purple curve, T2) and 52 °C after (red curve, T3) the sample. Heat loss may explain these differences, as the sensors T1 and T2 are positioned a few meters after the heater, and insulated with 3 cm of Armaflex insulator (k = 0.035 W/m/°C).

After the dehydration of the material, the heater was stopped, resulting in a decrease in the temperature (cooling step, green rectangle). For probes T1 and T2, located before the reactor, the room temperature was reached after about 3 h, while 24 h were needed for sensors T3 and T4, located after the reactor.

The material was finally humidified by a mix of nitrogen and water vapor (blue rectangle), with an input relative humidity of about 60 % RH. Thermochemical energy from this hydration of the material

Table 3
Energy release for physical sorption.

	Quantity of energy released (MJ)	% of theoretical energy released
Experimental value	1.83	10.7
Theoretical value	17.06	100

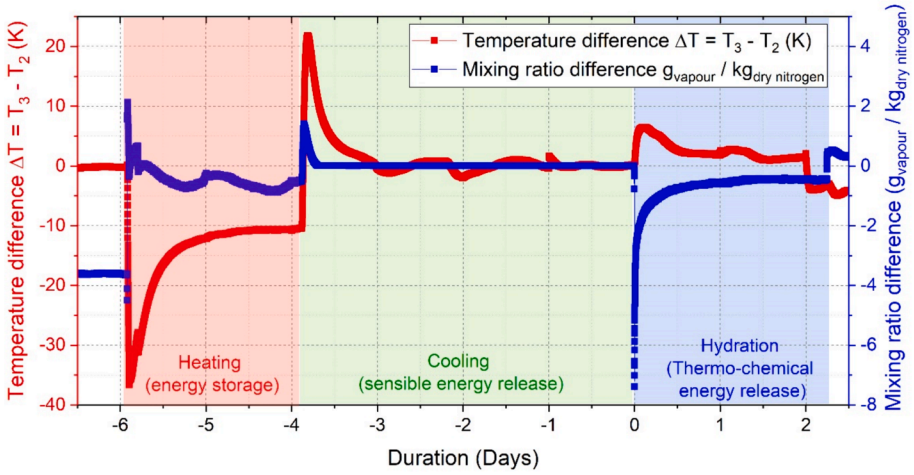

Fig. 10. Temperature difference (red line) and mixing ratio of water vapor (blue line) through the reactor.

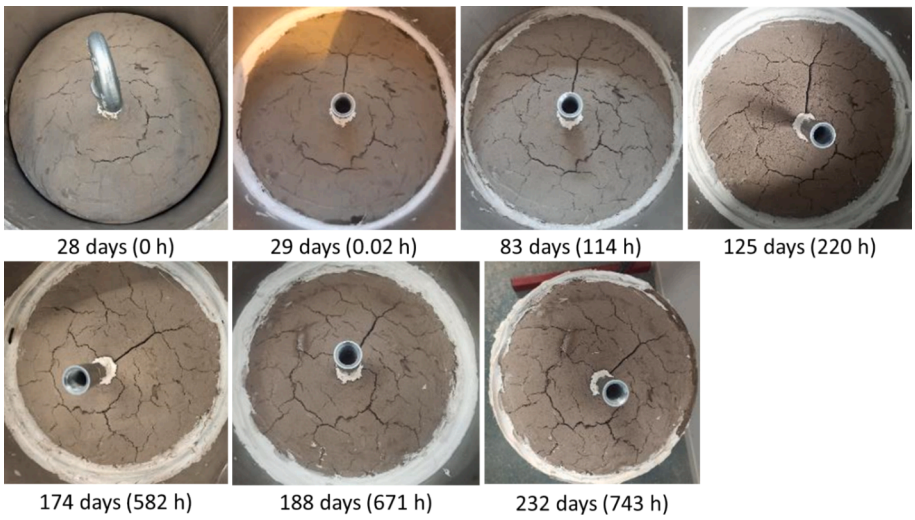

Fig. 11. Picture of the upper surface of cementitious materials at different times from casting (with the number of hours spent under nitrogen flow in parentheses).

increased the gas flow temperature after the reactor. The mixing ratio in the downstream flow was increased from 0 to 3.2 $g_{vapor}/kg_{dry\ nitrogen}$ within 2 h (Fig. 8 (b)). After one day, the relative humidity and the temperature difference were stabilized, making the release of energy negligible compared to heating from room temperature. Fig. 8 (c) presents the corresponding evolution of flow rate and pressure P1 for the corresponding time.

Fig. 9 focuses on the temperature variation during the hydration step. The prototype was stopped after more than two days when the upstream (T2) and downstream (T3) temperatures were similar.

4.1.2. Focus on the thermal energy discharge step

It can be seen from Fig. 9 that the temperatures recorded by probes T1 and T2 (before the reactor) decreased by 3 K. This sudden drop could be explained by two effects: the water evaporation when injected in the network, consistent with adiabatic humidification, and the gas origin (the gas is taken outside, where the temperature is lower than in the prototype room). The resulting temperature of adiabatic humidification from gas at 0 %RH (19 °C) to 58 %RH would be 8.8 K.

On the other side of the reactor, the gas flow temperature after crossing the storage material was increased by three degrees to reach 22 °C, which was 6 K more than the inlet temperature. As the temperature in T3 and T4 was higher than the room temperature (+2 K), it was deduced that this increase was not due to external heating from the room but by the production of heat from the transformation of meta-ettringite to ettringite within the storage material.

After 0.5 days, a drop in the temperature was observed for the downstream sensors (T3 and T4) from room temperature. This may be due to a colder gas flow, as the outside temperature moved from 22 °C at t = 0 to 10 °C at 0.75 days. From this moment, supplementary heating may have come from the room, as a temperature increase was observed in the hose (T4 > T3). Better insulation would help to distinguish between heating from the material and that due to a rise in room temperature.

4.1.3. Measurement of energy release in downstream flow

Based on temperature and humidity evaluation in the third step (hydration), the energy released could be calculated. Fig. 10 gathers

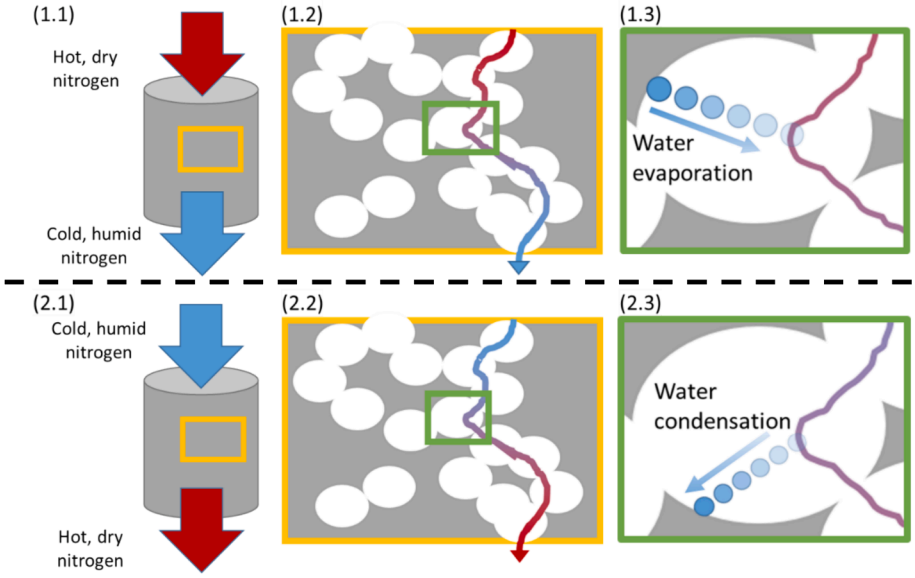

Fig. 12. Description of the evaporation/condensation phenomena during the heating and hydration steps, respectively. (1.1) Full-scale foam storage material; (1.2) Gas flow path within porosities of the foam and (1.3) Physical desorption of water (evaporation) as energy is provided by the hot nitrogen flow. (2.1), (2.2), and (2.3) are similar representations of the phenomena occurring during hydration with the physical sorption of water in porosities.

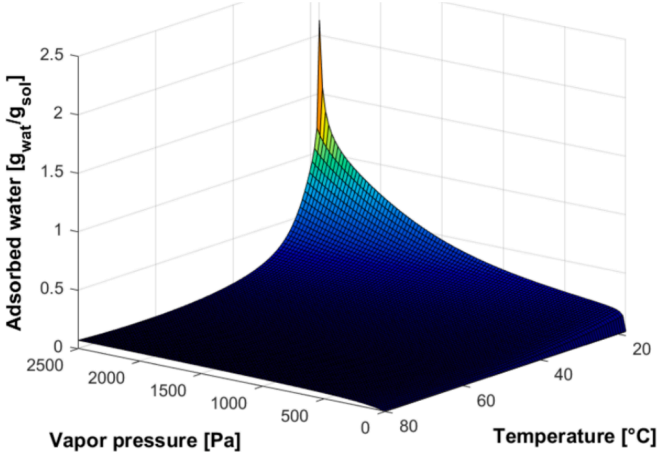

Fig. 13. Water sorption isotherm of ettringite from the model by Pickett et al. [61].

together the temperature (T3-T2) and mixing ratio of vapor variations between the reactor outlet and inlet for the entire process. With a particular focus on the release of energy from 0 to 2 days, the quantity of energy released could be determined from Eq. (A. 1).

About mixing ratio, the difference is negative during the heating step which is inconsistent with drying, but may be explained by very low values (below 10 %RH before and after) leading to a lack of precision of the sensor.

A difference of 6.5 K from the input to the output could be found after 2 h. Calculating temperature difference based on the specific heat of 1260 $J.kg^{-1}.K^{-1}$ (see section 3.2) gives a power released of about 1.83 MJ (509 kWh) or 45 MJ/m^3.

Considering a similar temperature variation for the reactor edges, made of 304-L stainless steel (with a mass of 140 kg and a heat capacity of 500 J/kg/K), suggests that these edges would store about 0.45 MJ.

As presented in the appendix, this experimental determination could be compared with the theoretical value from Eq. (A. 1) to Eq. (A. 9). The mass of ettringite was determined as 23.5 kg from Eq. (1), based on 30 kg of cement and 12.8 kg of water, excluding other products. The theoretical energy for physical sorption (water condensation) was calculated as 14.5 MJ (2.39 kJ/g_{water}), with an energy density of 2.57 MJ (0.42 kJ/g_{water}) for the chemical reaction [56]. Twenty molecules of water were considered to react with meta-ettringite to form ettringite (see Eq. (2)), corresponding to 6 kg of water. Results for physical sorption are given in Table 3. From this table, the experimental value of 1.83 MJ represents 10 % of the theoretical values. Some progress would still be needed to reach the performance of other experimental benches from Table 1. However, this sample was a monolith of the material; others were generally powder. This difference led to some engineering issues that will be discussed in the next section.

Table 4
Theoretical and experimental mass of water stored by the ettringitic material.

Mass of water stored experimentally (Eq. (5))	Mass of water theoretically stored (Fig. 14)		Mass of water that theoretically reacts (Table 3)
$m_{water}/m_{ettringite}$ (kg_{water}/kg_{cement})	Partial pressure of water (Pa)	Absorbed water (g_{water}/g_{sol}) Picket	Theoretical reacting water
$\frac{0.475}{23.5} = 0.020$	939	0.3077	$\frac{m_{water}}{m_{monolith}} = \frac{6.0}{23.5} = 0.26$

4.2. Discussion

Previous experiments [7], using a 6.5 dm^3 sample to store 426 MJ/m^3, led to the development of the prototype presented in this study, able to store 43 MJ/m^3 in a scaled-up sample (43 dm^3). This scale-up leads to several issues that may explain this decrease in energy storage capacity, such as a lower porosity, a lower humidity ratio at the inlet, or a possible carbonation.

4.2.1. Decrease of the accessibility to the material due to preferential paths

The new samples of 43 dm^3 involved a height of 50 cm, while that of previous samples was about 20 cm. This higher specimen led to a more critical coalescence of the gas bubbles (see section 3.2) and the collapse of the monolith for similar porosity. Thus, porosity was decreased from 76 % in low-scale samples to 53 % for this prototype. This reduction led to a lower gas permeability in the cementitious material, from 4 to 1 × 10^{-12} m^2. During experiments, cracks started to appear in the material, as illustrated in Fig. 11. They might be due to shrinkage from the drying of cementitious material.

These cracks would promote the presence of preferential flow paths through the cementitious material. These paths, which drive the

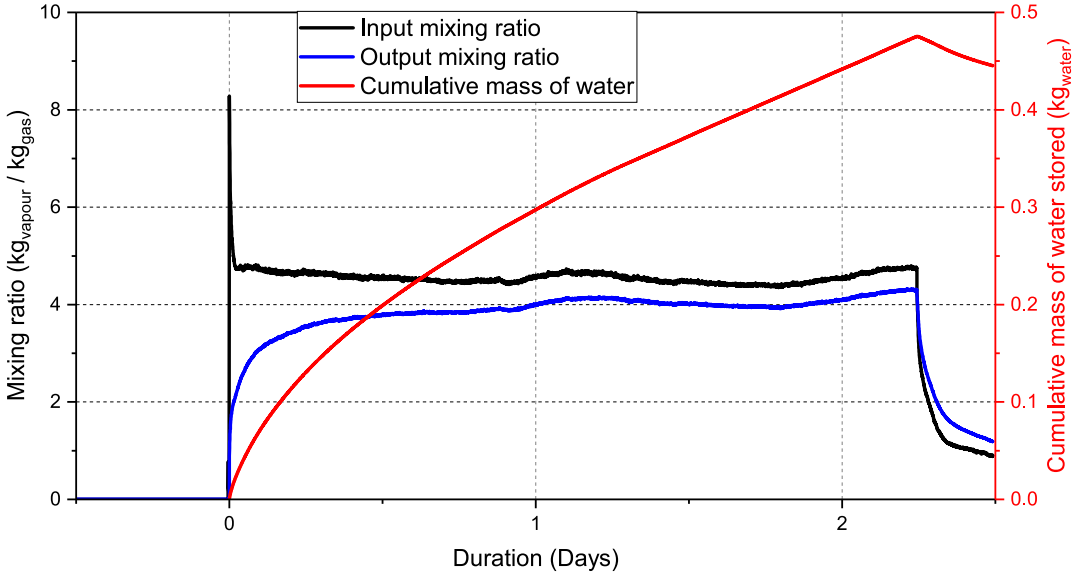

Fig. 14. Mixing ratio at input and output of the reactor and cumulative mass of water stored in cementitious material.

dehydration of cement by heating, and its rehydration are schematized in Fig. 12. Due to such paths, the gas flow meets only a few pores and it is assumed that the rest of the material does not undergo transformation into meta-ettringite and so does not take part in the energy storage process.

The cracks evolution is assumed to come from mechanical constraints created by the pressured airflow on the material, due to its low mechanical resistance. Another assumption is the volume change due to chemical reactions: with the water during the energy storage process or with the carbon during the carbonation process.

For several prototypes presented in Table 1, the reactive material volume change during storage cycling was an important issue. At the laboratory prototype scale, the reaction reversibility was measured through mass measurement: mass gain was quantified using a weight scale [47] on three samples at operational conditions for several cycles (7 cycles for 42 days). The results showed that 98 % of the mass was recovered and no material damage was detected. The low energy released presented in Table 3, and thus the low part of the material reacted, could conceal a concern due to volume change at the large-scale prototype.

4.2.2. Low relative humidity before the prototype

The quantity of water absorbed by the cementitious material is driven by the vapor pressure, as presented by Pickett's model (see Fig. 13). According to Eq. (A. 6), such vapor pressure depends on relative humidity, an increase of which would therefore raise the quantity of absorbed water [60].

Only 60 %RH at 15.5 °C (vapor pressure p_v of 1090 Pa) could be reached in the gas flow before it arrived at the material (see Figure A. 4), leading to absorption of only 0.36 $g_{water}/g_{material}$. Increasing the input humidity to 100 % RH at 15.5 °C (p_v = 1760 Pa) with a better system would raise the quantity of water absorbed to 0.79 $g_{water}/g_{material}$ and thus raise the amount of energy released by the material.

4.2.3. Accessibility of water to the dehydrated material

From the previous paragraphs, it appears that the chemical reaction needed the adsorption of water by the dehydrated material. It was assumed that the quantity of water absorbed by the material depended on the difference in mixing ratio between the input and output of the reactor, following Eq. (7).

$$m_{water} = (w_3 - w_2) \times Q_{dtf} \times \rho_{dtf} \times \Delta t \quad (7)$$

with m_{water} the mass (kg) of water, w_2 and w_3 the mixing ratios, respectively before and after the reactor (kg_{vapor}/kg_{dtg}), Δt the time difference between two measurement (s), Q_{dtf} and ρ_{dtf} the flow and density of the heat transport gas, respectively. The cumulated amount of water absorbed by the material is presented in Fig. 14.

At the end of the experiment, about 0.475 kg of water had been stored in 23 kg of cementitious material. This result is compared to theoretical values in Table 4

. The first observation that can be made from this table is the significant difference between experimental and theoretical values (about 10 %). This value is similar to the relation between theoretical and experimental values for energy measurement in Table 3, based on temperature measurement. The increase in contact surface by limiting the preferential paths might be a key factor in improving water adsorption and energy release. A compromise has to be found to limit the collapse of the material with too low porosity.

4.2.4. Additional explanation: carbonation

Ettringite is subject to carbonation, as previously described in Section 2.4. The cementitious monolith was surrounded by nitrogen during experiments but surrounded by air when the prototype was stopped (usually one week per month for maintenance or replacement of the monolith). In contact with carbon dioxide, ettringite would change into calcite, reducing the quantity of material able to store energy. Chen et al. found that the ettringite material was carbonated after about 1000 h under a 1 % CO_2 atmosphere and 55–95 %RH [51]. Xiantuo et al. [52] left ettringite under a CO_2 concentration closer to ambient conditions (0.06 % of CO_2) at 20 °C and different water vapor pressures. For dry flow (p_v = 27 Pa), no carbonation was found, while 30 % of ettringite was carbonated after 4 h in air saturated with vapor (p_v = 1760 Pa). From the equations given by the authors, a carbonation of 10 % could be expected after 4 h of hydration (p_v = 1090 Pa) in contact with air (0.04 % of CO_2). The different data could not confirm or refute the ability of the monolith to be carbonated, which will need to be clarified by a deeper study. Even though the material has been tested in the literature as a powder with higher activity, the type of carbonation evoked here has to be considered.

5. Conclusion

The reaction between meta-ettringite and water vapor is known to release a large quantity of thermochemical energy in a repeatable way. This reaction allowed a storage system to be built that operated by dehydrating the ettringite, keeping the material insulated from water vapor, and releasing the energy on demand. However, no open-system prototype has ever been developed to demonstrate this ability on an industrial scale. The prototype developed for this study presented a new and innovative way to study the energy stored in a cementitious material at an industrial scale. The following properties are found for the scaled-up material:

- A density of 869 kg/m^3 was found as an optimization of accessibility to the material while avoiding coalescence.
- A mechanical strength result of about 3.5 MPa showed that a monolith of the material could be considered as a self-supporting wall.
- An experimental energy release of about 43 MJ/m^3, about 10 % of theoretical values.

This gap with theoretical value is due to a low water absorption by the material. Engineering work needs to be continued to solve some issues and increase the efficiency of this prototype even more. The key factors for storing a higher quantity of energy seem to be:

- An increase in the inlet mixing ratio;
- Homogeneous distribution of porosities to avoid preferential paths;
- A permanent nitrogen flow to limit the carbonation.

CRediT authorship contribution statement

Noé Beaupere: Writing – original draft, Visualization, Validation, Methodology, Investigation, Formal analysis, Data curation. **Alexandre Malley-Ernewein:** Writing – review & editing, Visualization, Methodology, Formal analysis. **Tamar Nahhas:** Writing – original draft. **Stéphane Ginestet:** Writing – review & editing, Supervision, Resources, Project administration, Funding acquisition, Conceptualization. **Gabriel Samson:** Writing – review & editing, Methodology. **Martin Cyr:** Writing – review & editing, Funding acquisition, Conceptualization.

Declaration of competing interest

The authors declare that they have no known competing financial interests or personal relationships that could have appeared to influence the work reported in this paper.

Acknowledgments

This work is financially supported by the Occitanie Region (France) in the framework of the PROTEuS (PROTotype Energy Storage) project,

Programme opérationnel FEDER-FSE Midi-Pyrénées et AGaronne 2014-2020. The authors also thank Toulouse Tech Transfer for their financial support.

Appendix A. Supplementary material

Supplementary data to this article can be found online at https://doi.org/10.1016/j.solener.2024.112927.

References

[1] J. Lizana, R. Chacartegui, A. Barrios-Padura, J.M. Valverde, Advances in thermal energy storage materials and their applications towards zero energy buildings: a critical review, Appl. Energy 203 (2017) 219–239, https://doi.org/10.1016/j.apenergy.2017.06.008.

[2] D. Laing, D. Lehmann, C. Bahl, 'Concrete storage for solar thermal power plants and industrial process heat', in *Third International Renewable Energy Storage Conference (IRES 2008)*, Berlin, Nov. 2008. Accessed: Dec. 15, 2023. [Online]. Available: https://elib.dlr.de/57976/.

[3] D. Laing, C. Bahl, T. Bauer, D. Lehmann, W.-D. Steinmann, Thermal energy storage for direct steam generation, Sol. Energy 85 (4) (2011) 627–633, https://doi.org/10.1016/j.solener.2010.08.015.

[4] D. Laing, C. Bahl, T. Bauer, M. Fiss, N. Breidenbach, M. Hempel, High-temperature solid-media thermal energy storage for solar thermal power plants, Proc. IEEE 100 (2) (2012) 516–524, https://doi.org/10.1109/JPROC.2011.2154290.

[5] D. Laing, W.-D. Steinmann, R. Tamme, C. Richter, Solid media thermal storage for parabolic trough power plants, Sol. Energy 80 (10) (2006) 1283–1289, https://doi.org/10.1016/j.solener.2006.06.003.

[6] D. Laing, D. Lehmann, M. Fiß, C. Bahl, 'Test Results of Concrete Thermal Energy Storage for Parabolic Trough Power Plants', *J. Sol. Energy Eng.*, 131(4) (2009), doi: 10.1115/1.3197844.

[7] K. Ndiaye, M. Cyr, S. Ginestet, Development of a cementitious material for thermal energy storage at low temperature, Constr. Build. Mater. 242 (2020) 118130, https://doi.org/10.1016/j.conbuildmat.2020.118130.

[8] K. Ndiaye, S. Ginestet, M. Cyr, Experimental evaluation of two low temperature energy storage prototypes based on innovative cementitious material, Appl. Energy 217 (2018) 47–55, https://doi.org/10.1016/j.apenergy.2018.02.136.

[9] J.-C. Hadorn, *Thermal energy storage for solar and low energy buildings - State of the art*, IEA. in IEA Solar Heating and Cooling Task 32. 2005.

[10] A. Kur, J. Darkwa, J. Calautit, R. Boukhanouf, and M. Worall, 'Solid–Gas Thermochemical Energy Storage Materials and Reactors for Low to High-Temperature Applications: A Concise Review', *Energies*, vol. 16, no. 2, Art. no. 2, Jan. 2023, doi: 10.3390/en16020756.

[11] M. Boucher, F. Streiff, 'La chaleur fatale', ADEME, Sep. 2017. Accessed: Aug. 27, 2024. [Online]. Available: https://librairie.ademe.fr/energies-renouvelables-reseaux-et-stockage/2312-chaleur-fatale.html.

[12] R. Salgado-Pizarro, A. Calderón, A. Svobodova-Sedlackova, A.I. Fernández, C. Barreneche, The relevance of thermochemical energy storage in the last two decades: the analysis of research evolution, J. Energy Storage 51 (2022) 104377, https://doi.org/10.1016/j.est.2022.104377.

[13] J. Xu, R.Z. Wang, Y. Li, A review of available technologies for seasonal thermal energy storage, Sol. Energy 103 (2014) 610–638, https://doi.org/10.1016/j.solener.2013.06.006.

[14] C. Bales *et al.*, *Laboratory Tests of Chemical Reactions and Prototype Sorption Storage Units : Report B4 of Subtask B*. IEA-SHC, 2008. Accessed: Dec. 16, 2020. [Online]. Available: http://urn.kb.se/resolve?urn=urn:nbn:se:du-3373.

[15] C. Bales, S. Nordlander, 'TCA Evaluation; Lab Measurements, Modelling and System Simulations,'' Solar Energy Research Center, ISSN 1401 – 7555, ISRN DU-SERC–91—SE', Dec. 2005.

[16] R. Weber, V. Dorer, Long-term heat storage with NaOH, Vacuum 82 (7) (2008) 708–716, https://doi.org/10.1016/j.vacuum.2007.10.018.

[17] D. Jaehnig, R. Hausner, W. Wagner, C. Isaksson, 'Thermo-chemical storage for solar space heating in a single-family house', in *Ecostock conference*, Stockton N.,J., 2006, p. 7.

[18] S. Mauran, H. Lahmidi, V. Goetz, Solar heating and cooling by a thermochemical process. first experiments of a prototype storing 60kWh by a solid/gas reaction, Sol. Energy 82 (7) (2008) 623–636, https://doi.org/10.1016/j.solener.2008.01.002.

[19] Y.J. Zhao, R.Z. Wang, T.X. Li, Y. Nomura, Investigation of a 10 kWh sorption heat storage device for effective utilization of low-grade thermal energy, Energy 113 (2016) 739–747, https://doi.org/10.1016/j.energy.2016.07.100.

[20] T. Yan, H. Zhang, N. Yu, D. Li, Q.W. Pan, Performance of thermochemical adsorption heat storage system based on MnCl2-NH3 working pair, Energy 239 (2022) 122327, https://doi.org/10.1016/j.energy.2021.122327.

[21] M.M. Salama, S.A. Mohamed, M. Attalla, A.N. Shmroukh, Experimental investigation on a thermochemical seasonal sorption energy storage battery utilizing MgSO4-H2O, Environ. Sci. Pollut. Res. 30 (43) (2023) 98502–98525, https://doi.org/10.1007/s11356-023-28875-1.

[22] A. Ahmad, Y. Ding, A thermochemical energy storage based cooling and heating system: modelling, experimental validation and lab-scale demonstration, Energy Convers. Manag. 247 (2021) 114748, https://doi.org/10.1016/j.enconman.2021.114748.

[23] A. A. Hawwash, S. Mori, H. Hassan, 'An experimental investigation on the performance of designed closed reactor system on the thermochemical heat storage of magnesium chloride hexahydrate', *Exp. Heat Transf.*, vol. 0, no. 0, pp. 1–20, doi: 10.1080/08916152.2023.2240807.

[24] T. Yan, Z.H. Kuai, S.F. Wu, Experimental investigation on a MnCl2–SrCl2/NH3 thermochemical resorption heat storage system, Renew. Energy 147 (2020) 874–883, https://doi.org/10.1016/j.renene.2019.09.033.

[25] T. Yan, T. Xie, W.G. Pan, L.W. Wang, Experimental study on ammonia-based thermochemical resorption thermal energy storage system, Renew. Energy 229 (2024) 120696, https://doi.org/10.1016/j.renene.2024.120696.

[26] X. Han, S. Liu, C. Zeng, L. Yang, A. Shukla, Y. Shen, Investigating the performance enhancement of copper fins on trapezoidal thermochemical reactor, Renew. Energy 150 (2020) 1037–1046, https://doi.org/10.1016/j.renene.2019.11.052.

[27] L. Farcot, N. Le Pierrès, J.-F. Fourmigué, Experimental investigation of a moving-bed heat storage thermochemical reactor with SrBr 2/H2O couple, J. Energy Storage 26 (2019) 101009, https://doi.org/10.1016/j.est.2019.101009.

[28] B. Michel, N. Mazet, S. Mauran, D. Stitou, J. Xu, Thermochemical process for seasonal storage of solar energy: Characterization and modeling of a high density reactive bed, Energy 47 (1) (2012) 553–563, https://doi.org/10.1016/j.energy.2012.09.029.

[29] B. Michel, N. Mazet, P. Neveu, Experimental investigation of an innovative thermochemical process operating with a hydrate salt and moist air for thermal storage of solar energy: global performance, Appl. Energy 129 (2014) 177–186, https://doi.org/10.1016/j.apenergy.2014.04.073.

[30] H. Zondag, B. Kikkert, S. Smeding, R. de Boer, M. Bakker, Prototype thermochemical heat storage with open reactor system, Appl. Energy 109 (2013) 360–365, https://doi.org/10.1016/j.apenergy.2013.01.082.

[31] A. Mukherjee, et al., Performance assessment of open thermochemical energy storage system for seasonal space heating in highly humid environment, Renew. Energy 201 (2022) 204–223, https://doi.org/10.1016/j.renene.2022.10.075.

[32] M. K. John, K. Vishnu, C. Vishnu, B. Rohinikumar, C. Muraleedharan, 'Experimental and numerical investigations on an open thermochemical energy storage system using low-temperature hydrate salt', *Therm. Sci. Eng. Prog.*, 53 (2024) 102749, doi: 10.1016/j.tsep.2024.102749.

[33] Y.N. Zhang, R.Z. Wang, T.X. Li, Experimental investigation on an open sorption thermal storage system for space heating, Energy 141 (2017) 2421–2433, https://doi.org/10.1016/j.energy.2017.12.003.

[34] H. Zhang, T. Yan, N. Yu, C.Y. Wang, Experimental investigation on a strontium chloride/ammonia sorption heat storage system, Appl. Therm. Eng. 219 (2023) 119478, https://doi.org/10.1016/j.applthermaleng.2022.119478.

[35] H. Yang, et al., Experimental investigation of a thermochemical energy storage system based on MgSO4-silica gel for building heating: adsorption/desorption performance testing and system optimization, Energy Convers. Manag. 301 (2024) 118000, https://doi.org/10.1016/j.enconman.2023.118000.

[36] J. Wyttenbach, et al., Performances and modelling of a circular moving bed thermochemical reactor for seasonal storage, Appl. Energy 230 (2018) 803–815, https://doi.org/10.1016/j.apenergy.2018.09.008.

[37] S. Koley, H. Bao, A.P. Roskilly, Z. Ma, Experimental parametric evaluation of adsorption characteristics for silica gel - water based open-bed system for seasonal thermal energy storage, J. Energy Storage 89 (2024) 111812, https://doi.org/10.1016/j.est.2024.111812.

[38] C. Strong, Y. Carrier, and F. Handan Tezel, 'Experimental optimization of operating conditions for an open bulk-scale silica gel/water vapour adsorption energy storage system', Appl. Energy, 312 (2022) 118533, doi: 10.1016/j.apenergy.2022.118533.

[39] X. Liu, X. Liu, F. Yang, Y. Wu, Experimental investigation of low-temperature fluidised bed thermochemical energy storage with salt-mesoporous silica composite materials, Appl. Energy 362 (2024) 122953, https://doi.org/10.1016/j.apenergy.2024.122953.

[40] S. Hongois, F. Kuznik, P. Stevens, J.-J. Roux, Development and characterisation of a new MgSO4−zeolite composite for long-term thermal energy storage, Sol. Energy Mater. Sol. Cells 95 (7) (2011) 1831–1837, https://doi.org/10.1016/j.solmat.2011.01.050.

[41] M. Gaeini, R. van Alebeek, L. Scapino, H.A. Zondag, C.C.M. Rindt, Hot tap water production by a 4 kW sorption segmented reactor in household scale for seasonal heat storage, J. Energy Storage 17 (2018) 118–128, https://doi.org/10.1016/j.est.2018.02.014.

[42] R. van Alebeek, L. Scapino, M.A.J.M. Beving, M. Gaeini, C.C.M. Rindt, H. A. Zondag, Investigation of a household-scale open sorption energy storage system based on the zeolite 13X/water reacting pair, Appl. Therm. Eng. 139 (2018) 325–333, https://doi.org/10.1016/j.applthermaleng.2018.04.092.

[43] R.-J. Clark, M. Farid, Experimental investigation into cascade thermochemical energy storage system using SrCl2-cement and zeolite-13X materials, Appl. Energy 316 (2022) 119145, https://doi.org/10.1016/j.apenergy.2022.119145.

[44] F. Winnefeld, J. Kaufmann, 'Concrete produced with calcium sulfoaluminate cement – a potential system for energy and heat storage', in *First Middle East Conference on Smart Monitoring, Assessment and Rehabilitation of Civil Structures,* Dubai, United Arab Emirates, Feb. 2011.

[45] J. Kaufmann, F. Winnefeld, Seasonal heat storage in calcium sulfoaluminate based hardened cement pastes – experiences with different prototypes, J. Energy Storage 25 (2019) 100850, https://doi.org/10.1016/j.est.2019.100850.

[46] B. Chen, 'Study of an ettringite-based thermochemical energy storage for buildings', Ph.D. Thesis, Lyon, 2020. Accessed: Aug. 10, 2022. [Online]. Available: https://www.theses.fr/2020LYSEI056.

[47] K. Ndiaye, M. Cyr, S. Ginestet, Durability and stability of an ettringite-based material for thermal energy storage at low temperature, Cem. Concr. Res. 99 (2017) 106–115, https://doi.org/10.1016/j.cemconres.2017.05.001.

[48] B. Chen, F. Kuznik, M. Horgnies, K. Johannes, V. Morin, E. Gengembre, Physicochemical properties of ettringite/meta-ettringite for thermal energy storage: review, Sol. Energy Mater. Sol. Cells 193 (2019) 320–334, https://doi.org/10.1016/j.solmat.2018.12.013.
[49] L.J. Struble, P.W. Brown, Heats of dehydration and specific heats of compounds found in concrete and their potential for thermal energy storage, Sol. Energy Mater. 14 (1) (1986) 1–12, https://doi.org/10.1016/0165-1633(86)90008-0.
[50] F. Winnefeld, J. P. Kaufmann, 'Concrete produced with calcium sulfoaluminate cement – a potential system for energy and heat storage', p. 8.
[51] B. Chen, M. Horgnies, B. Huet, V. Morin, K. Johannes, F. Kuznik, Comparative kinetics study on carbonation of ettringite and meta-ettringite based materials, Cem. Concr. Res. 137 (2020) 106209, https://doi.org/10.1016/j.cemconres.2020.106209.
[52] C. Xiantuo, Z. Ruizhen, C. Xiaorong, Kinetic study of ettringite carbonation reaction, Cem. Concr. Res. 24 (7) (1994) 1383–1389, https://doi.org/10.1016/0008-8846(94)90123-6.
[53] T. Nishikawa, K. Suzuki, S. Ito, K. Sato, T. Takebe, Decomposition of synthesized ettringite by carbonation, Cem. Concr. Res. 22 (1) (1992) 6–14, https://doi.org/10.1016/0008-8846(92)90130-N.
[54] T. Grounds, H.G. Midgley, D.V. Novell, Carbonation of ettringite by atmospheric carbon dioxide, Thermochim. Acta 135 (1988) 347–352, https://doi.org/10.1016/0040-6031(88)87407-0.
[55] Q. Zhou, F.P. Glasser, Thermal stability and decomposition mechanisms of ettringite at <120°C, Cem. Concr. Res. 31 (9) (2001) 1333–1339, https://doi.org/10.1016/S0008-8846(01)00558-0.
[56] K. Ndiaye, 'Etude numérique et expérimentale du stockage d'énergie par les matériaux cimentaires', phd, Université de Toulouse, Université Toulouse III - Paul Sabatier, 2016. Accessed: Oct. 19, 2020. [Online]. Available: http://thesesups.ups-tlse.fr/3354/.
[57] *NF P18-459 Concrete - Testing hardened concrete - Testing porosity and density*, Mar. 2010. [Online]. Available: https://www.boutique.afnor.org/en-gb/standard/nf-p18459/concrete-testing-hardened-concrete-testing-porosity-and-density/fa160729/34961#AreasStoreProductsSummaryView.
[58] T. Honorio, Thermal conductivity, heat capacity and thermal expansion of ettringite and metaettringite: effects of the relative humidity and temperature, Cem. Concr. Res. 159 (2022) 106865, https://doi.org/10.1016/j.cemconres.2022.106865.
[59] 'ISO 1217:2009(fr), Compresseurs volumétriques — Essais de réception'. Accessed: Nov. 28, 2022. [Online]. Available: https://www.iso.org/obp/ui/#iso:std:iso:1217:ed-4:v1:fr.
[60] G. Pickett, Modification of the Brunauer—Emmett—Teller theory of multimolecular adsorption, J. Am. Chem. Soc. 67 (11) (1945) 1958–1962, https://doi.org/10.1021/ja01227a027.
[61] 'WebBook de Chimie NIST, SRD 69', National Institut Of Standards and Technologie - U.S. Department of Commerce - Webbook. Accessed: Dec. 08, 2021. [Online]. Available: https://webbook.nist.gov/cgi/cbook.cgi?ID=C7732185&Mask=4&Type=ANTOINE&Plot=on#ANTOINE.
[62] L. Borel, D. Favrat, *Thermodynamique et énergétique*, 2nd edition. in Mécanique. PPUR presses polytechniques, 2005. [Online]. Available: https://www.epflpress.org/produit/332/9782880745455/thermodynamique-et-energetique-volume-1.